coatings

MDPI

Article

Compositional Engineering of $FAPbI_3$ Perovskite Added MACl with $MAPbBr_3$ or $FAPbBr_3$

Sung Hwan Joo and Hyung Wook Choi *

Department of Electrical Engineering, Gachon University, 1342 Seongnam Daero, Seongnam-si 13120, Korea; joo8896@gachon.ac.kr

* Correspondence: chw@gachon.ac.kr; Tel.: +82-31-750-5562

Abstract: Many attempts have been made to stabilize α-phase formamidinium lead iodide (α-$FAPbI_3$) using mixed cations or anions with MA^+, FA^+, Br^- and I^-. A representative method is to stably produce α-$FAPbI_3$ by adding methylammonium lead ($MAPbBr_3$) to the light absorption layer of a perovskite solar cell and using methylammonium chloride (MACl) as an additive. However, in the perovskite containing MA^+ and Br^-, the current density is lowered due to an unwanted increase in the bandgap; phase separation occurs due to the mixing of halides, and thermal stability is lowered. Therefore, in this study, in order to minimize the decrease in the composition ratio of $FAPbI_3$ and to reduce MA^+, the addition amount of MACl was first optimized. Thereafter, a new attempt was made to fabricate $FAPbI_3$ perovskite by using formamidinium lead bromide ($FAPbBr_3$) and MACl together as phase stabilizers instead of $MAPbBr_3$. As for the $FAPbI_3$-$MAPbBr_3$ solar cell, the $(FAPbI_3)_{0.93}(MAPbBr_3)_{0.07}$ device showed the highest efficiency. On the other hand, in the case of the $FAPbI_3$-$FAPbBr_3$ solar cell, the $(FAPbI_3)_{0.99}(FAPbBr_3)_{0.01}$ solar cell with a very small $FAPbBr_3$ composition ratio showed the highest efficiency with fast photovoltaic performance improvement and high crystallinity. In addition, the $FAPbI_3$-$FAPbBr_3$ solar cell showed a higher performance than the $FAPbI_3$-$MAPbBr_3$ solar cell, suggesting that $FAPbBr_3$ can sufficiently replace $MAPbBr_3$.

Keywords: Perovskite solar cells; $FAPbBr_3$; $FAPbI_3$; MACl

Citation: Joo, S.H.; Choi, H.W. Compositional Engineering of $FAPbI_3$ Perovskite Added MACl with $MAPbBr_3$ or $FAPbBr_3$. *Coatings* **2021**, *11*, 1184. https://doi.org/10.3390/coatings11101184

Academic Editor: Alessandro Latini

Received: 15 September 2021
Accepted: 27 September 2021
Published: 29 September 2021

1. Introduction

Perovskite solar cells (PSCs) are still one of the most popular fields and within a short period of time since their advent, they have achieved high power conversion efficiencies (PCEs) exceeding 25% with broader solar-light absorption through narrower bandgaps. Formamidinium lead iodide ($FAPbI_3$) has the narrowest bandgap (1.45–1.51 eV) among lead halide perovskites and improved thermal stability compared to methylammonium lead iodide [1,2]. However, α-$FAPbI_3$ (the $FAPbI_3$ perovskite) is prone to phase change to δ-$FAPbI_3$ (non-perovskite, hexagonal), which is thermodynamically more stable at room temperature. Yellow δ-$FAPbI_3$ reduces the crystallinity of the $FAPbI_3$ film, disrupting electron transport and reducing the performance of PSCs [3,4]. The first of two representative methods to overcome the phase transformation problem of α-$FAPbI_3$ is the use of methylammonium chloride (MACl) as an additive in the perovskite precursor solution. MACl induces the growth of the (001) plane of α-$FAPbI_3$ and improves the crystallinity of the perovskite [5,6]. Moreover, MACl can be removed by heating above 140 °C, which is essential for α-$FAPbI_3$ synthesis [7]. Therefore, a MA^+-free perovskite film can be produced using this method. The second method is to stably synthesize α-$FAPbI_3$ by adding methylammonium lead bromide ($MAPbBr_3$) with a cation smaller than FA^+ to the perovskite composition [8]. Researchers have focused primarily on mixed cations or anions in an effort to improve the stability of α-$FAPbI_3$. Therefore, $FAPbI_3$-$MAPbBr_3$ has been studied the most among all the processes for enhancing the phase stability of $FAPbI_3$ and exhibited a higher PCE than the first method of adding MACl. In addition, MACl has been used together in the manufacture of $FAPbI_3$-$MAPbBr_3$ perovskite, and here MACl has been

mainly used as 'a mediator for high-crystallinity'. However, this method has problems such as reduced light absorption, increased bandgap due to $MAPbBr_3$, and reduced thermal stability owing to MA^+ ions, resulting in a low current density [9]. Although we attempted to stabilize the α-$FAPbI_3$ phase without MA^+ using Rb^+ and Cs^+, the resulting PCE was still low when compared to the PCE obtained using FA^+ and MA^+ [10,11]. Therefore, to further improve the performance of PSCs, a novel configuration capable of stabilizing α-$FAPbI_3$ without MA^+ while controlling the bandgap increase inherent in $FAPbI_3$ is required.

We focused on the composition of mono-cation $FAPbI_3$-$FAPbBr_3$ perovskite, which can help improve α-$FAPbI_3$ phase stability. However, δ-$FAPbI_3$ was still found in the $FAPbI_3$-$FAPbBr_3$ film, resulting in poor solar cell performance. In this study, a new attempt was made to solve this problem by using MACl as an additive to increase the phase stability of α-$FAPbI_3$ together with $FAPbBr_3$. The combination of cations and anions added to the perovskite is important to improve the stability of $FAPbI_3$ [12]. Therefore, $FAPbI_3$-$FAPbBr_3$ with MACl added stably produced α-$FAPbI_3$ by combining MA^+ and Br^-. In addition, α-$FAPbI_3$ films are stably fabricated by the formation of metastable two-dimensional $MAFAPbI_3Cl$ perovskite intermediates with high free energy due to the Cl- in the precursor solution [5]. The amount of MACl was first optimized and applied to the $FAPbI_3$ film, and then $MAPbBr_3$ or $FAPbBr_3$ was used in the perovskite composition. MACl added $FAPbI_3$-$FAPbBr_3$ films showed a dramatic improvement in photovoltaic performance even with very small amounts of $FAPbBr_3$. In addition, $FAPbI_3$-$FAPbBr_3$ PSCs showed a relatively high current density based on a smaller increase in $FAPbI_3$ intrinsic bandgap than $FAPbI_3$-$MAPbBr_3$ PSCs, suggesting that $FAPbBr_3$ could be used as a sufficient replacement for $MAPbBr_3$.

2. Materials and Methods

2.1. Materials

FTO glass (7 Ω sq-1, Wooyang GMS), titanium diisopropoxide bis(acetylacetone) (75 wt.% in isopropanol, Sigma-Aldrich, St. Louis, MO, USA), 1-butyl alcohol (99%, Sigma-Aldrich, St. Louis, MO, USA), TiO_2 paste (18 NR-T, Greatcell solar, Queanbeyan, Australia), N,N-dimethylformamide (DMF, 99.8%, Sigma-Aldrich, St. Louis, MO, USA), dimethyl sulfoxide (DMSO, ≥99.9%, Sigma-Aldrich, St. Louis, MO, USA), ethyl alcohol (≥99.5, Sigma-Aldrich, St. Louis, MO, USA), chlorobenzene (99.8%, Sigma-Aldrich, St. Louis, MO, USA), lead(II) iodide (99.999% trace metals basic, Sigma-Aldrich, St. Louis, MO, USA), lead(II) bromide (99.999% trace metals basic, Sigma-Aldrich, St. Louis, MO, USA), formamidinium iodide (FAI, greatcellsolar, Queanbeyan, Australia), methylammonium bromide (MABr, greatcellsolar, Queanbeyan, Australia), formamidinium bromide (FABr, greatcellsolar, Queanbeyan, Australia), methylammonium hydrochloride (MACl, greatcellsolar, Queanbeyan, Australia), toluene (99.9%, Sigma-Aldrich, St. Louis, MO, USA), 2,2′,7,7′-tetrakis[N,N-di(4-methoxyphenyl)amino]-9,9′-spirobifluorene (spiro-OMeTAD, 99%, Sigma-Aldrich, St. Louis, MO, USA), bis(trifluoromethane)-sulfonimide lithium salt (Li-TSFI; ≥99.0%, Sigma-Aldrich, St. Louis, MO, USA), acetonitrile (99.93%, Sigma-Aldrich, St. Louis, MO, USA), 4-tertbutylpyridine (98%, Sigma-Aldrich, St. Louis, MO, USA) were used. All reagents were used as received without further purification.

2.2. Device Preparation

FTO glass was used as the substrate for fabricating the device. The substrates were sequentially washed with acetone, ethanol, and deionized water for 15 min each in an ultrasonic bath. To deposit the compact-TiO_2 (c-TiO_2) layer, 55 mL of a titanium diisopropoxide bis (acetyl acetonate)/1-butyl alcohol (1:10 v/v) solution was spin-coated. The substrate was then heated at 120 °C for 15 min. On top of the c-TiO_2 layer, a mesoporous TiO_2 (mp-TiO_2) layer was spin-coated. TiO_2 paste with an average nanoparticle size of 20 nm was dispersed in ethyl alcohol (1:6 w/w). The prepared FTO/c-TiO_2/mp-TiO_2 substrates were calcined at 500 °C for 1 h and then cooled to room temperature. To fabricate the perovskite layer, 1.4 mol of perovskite solution was prepared in a mixture of DMF and

DMSO (8:1 *v*/*v*). MACl was then added to the prepared precursor solution. Each sample was spin-coated onto the mp-TiO_2 layer at 4000 rpm for 20 s. During the spin coating, 200 µL of toluene was added dropwise using a pipette after spinning for 10 s. The film was heated on a hot plate at 150 °C for 10 min. The hole transport layer was prepared using spiro-OMeTAD in chlorobenzene (72.3 mg/mL), and 28.8 µL 4-tert-butyl pyridine and 17.5 µL Li-bis solution (520 mg Li-TFSI/1 mL acetonitrile) were added. Finally, a 60 nm thick gold electrode was deposited using a thermal evaporation system.

2.3. Characterization and Device Measurement

UV-vis absorption spectra were measured using an Agilent 8453 UV-vis spectrophotometer (Agilent 8453, Agilent Technologies, Santa Clara, CA, USA) at a scan rate of 494.95 [nm/min] in the wavelength range 200–1000 nm. Phases of the perovskite films formed on FTO/TiO_2 were analyzed using an XRD Rigaku DMAX 2200 system (Rigaku, Tokyo, Japan) with Cu Kα radiation (λ = 0.1542 nm). XRD patterns were analyzed in five step sizes in the range 10–60° 2θ. The surfaces of the perovskite layer on the FTO/TiO_2 and the cross-sections of the FTO/TiO_2/perovskite/spiro-OMeTAD. were obtained using field-emission SEM (Hitachi S-4700, Tokyo, Japan). All SEM images were sputter coated with gold for conductivity and measured at an acceleration voltage of 15 kV and a probe current of 10 µA. All surface images were measured at 30k magnification at distances of 12.2 mm and 12.3 mm, and cross-sectional images were measured at 50k magnification at distances of 15.2 mm. J-V curves of the PSCs were measured using a solar simulator (Polaromix K201, Solar simulator LAB 50, McScience K3000, McScience, Gyeonggi-do, Korea) under one sun illumination (AM1.5G, 100 $mWcm^{-2}$). The active area of the PSCs was calculated using an area of 0.053 cm^{-2}.

3. Results and Discussion

3.1. $FAPbI_3$ Perovskite Solar Cells with MACl

To determine the optimal composition ratio of $MAPbBr_3$ and $FAPbBr_3$, five devices were prepared under various MACl conditions (0–50 mol%, or 0–50-MACl). Here, we designed a PSC with a fluorine-doped tin oxide (FTO)/TiO_2/perovskite/spiro-OMeTAD/Au structure. Figure 1a shows the current density-voltage (J-V) curves for the perovskite device for different amounts of MACl. A summary of the photovoltaic properties of 0–50-MACl PSCs is presented in Table 1. The device without MACl exhibited an open-circuit voltage (V_{OC}) of 0.831 V, a short-circuit current density (J_{SC}) of 16.696 $mAcm^{-2}$, a fill factor (FF) of 40.105%, and a PCE of 5.567%. The addition of MACl to the α-$FAPbI_3$ film increased the overall efficiency of all devices by stabilizing α-$FAPbI_3$ and improving the crystallinity [13]. The 40-MACl perovskite film exhibited the highest PCE of 15.379% with a V_{OC} of 0.908 V, a J_{SC} of 24.181 $mAcm^{-2}$, and an FF of 70.037%, indicating that the optimal MACl addition amount was 40 mol% (Table 1). However, as the MACl concentration increased to 50 mol%, the PCE decreased to 12.989%. The XRD pattern of the α-$FAPbI_3$ film (Figure 1b) by MACl concentration shows two characteristic peaks of α-$FAPbI_3$ at 13.95°, 24.26° and 28.12°, which are attributed to the (001) (111) (002) plane, along with one peak at 11.8° that corresponds to δ-$FAPbI_3$. In addition, the peak observed at 12.63° and 26.50° corresponds to lead iodide (PbI_2) residue due to incomplete reaction between PbI_2 and formamidinium iodide (FAI) in a perovskite precursor solution prepared by a stoichiometric method. The noticeable difference in the 2θ peak intensity of the α-$FAPbI_3$ (001) (002) plane shows an improvement of the crystallinity of the perovskite, which sharply increases with the increase of the MACl. In addition, the peak corresponding to δ-$FAPbI_3$ almost disappeared with the addition of MACl.

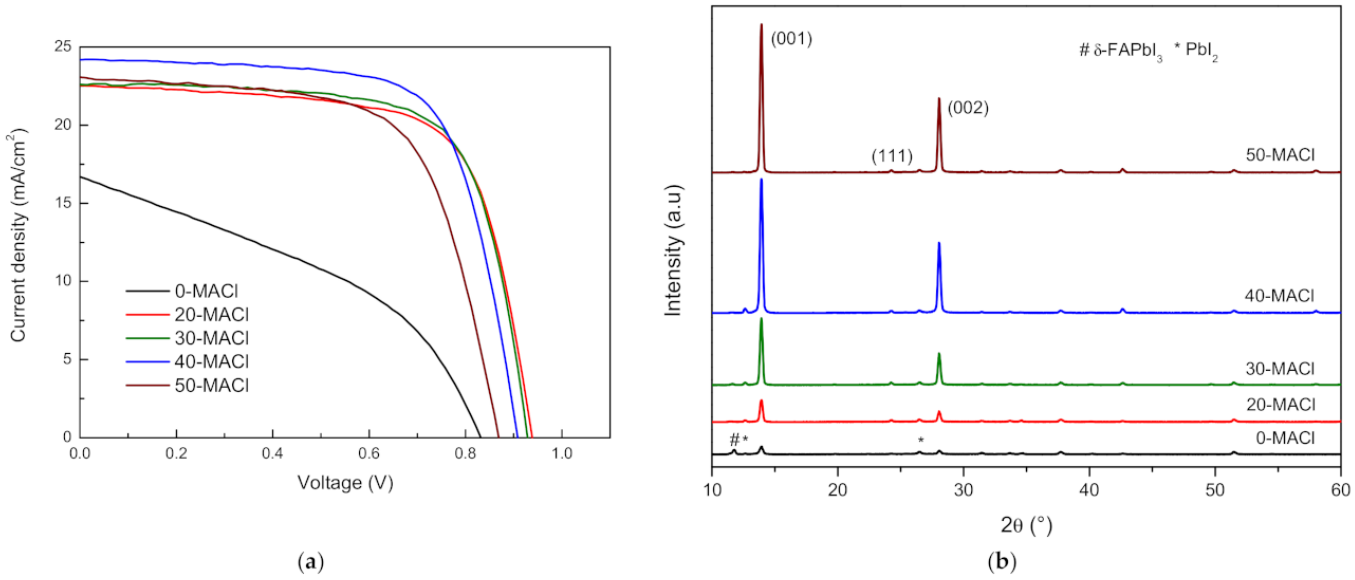

Figure 1. (**a**) Photocurrent density-voltage curve of the $FAPbI_3$ PSCs at different MACl concentrations.; (**b**) XRD patterns of the 0-, 20-, 30-, 40-, and 50-MACl perovskite films.

Table 1. Photovoltaic parameters of **the** best-performing $FAPbI_3$ PSCs with various amounts of MACl.

Sample	V_{OC}	J_{SC}	FF	PCE (%)	Rs(Ω)
0-MACl	0.831	16.696	40.105	5.567	331.839
20-MACl	0.938	22.550	68.982	14.596	119.269
30-MACl	0.929	22.599	70.791	14.859	104.548
40-MACl	0.908	24.181	70.037	15.379	109.747
50-MACl	0.869	23.074	64.768	12.989	135.155

3.2. $FAPbI_3$-$MAPbBr_3$ Perovskite Solar Cells

Using the optimized MACl condition, 12 devices were fabricated with various composition ratios of $MAPbBr_3$ and $FAPbBr_3$, which were used as light absorption layers to improve the phase stability of α-$FAPbI_3$ and improve the performance of PSCs. Figure 2a shows the J-V curves of the $(FAPbI_3)_{1-X}(MAPbBr_3)_X$ perovskite (renamed X-$MAPbBr_3$) device. A summary of the photovoltaic properties of the PSCs according to the composition ratio of $MAPbBr_3$ is presented in Table 2. The 0.07-$MAPbBr_3$ film exhibited the highest PCE of 16.301% with a V_{OC} of 1.017 V, a J_{SC} of 22.196 $mAcm^{-2}$, and an FF of 72.176%. In contrast, the PCE of the commonly used composition ratios, namely, 0.10-$MAPbBr_3$ and 0.15-$MAPbBr_3$, decrease gradually to 15.372% and 14.826%, respectively, which is attributed to the high series resistance (R_S) [14–17]. The existence of α-$FAPbI_3$ in the produced perovskite films was confirmed from the XRD pattern of the X-$MAPbBr_3$ film (Figure 2b), which also showed that the crystallinity of the perovskite film improved with increasing the amount of $MAPbBr_3$. However, as the composition ratio of $MAPbBr_3$ increased to 0.10 and 0.15, the perovskite crystallinity decreased. In addition, the α-$FAPbI_3$ peak shifted to a higher degree of diffraction with increasing amount of $MAPbBr_3$. Figure 2c shows the absorbance of the X-$MAPbBr_3$ perovskite film. The light absorption coefficient improved with the increasing amount of $MAPbBr_3$ in the X-$MAPbBr_3$ perovskite film. In particular, 0.07-$MAPbBr_3$ showed the highest absorbance. On the other hand, 0.10- and 0.15-$MAPbBr_3$ showed lower absorbance. When increasing the amount of $MAPbBr_3$, which has a wider bandgap than $FAPbI_3$ in the X-$MAPbBr_3$ perovskite film, the absorbance gradually blue-shifted in the 750–850 nm wavelength region [18,19].

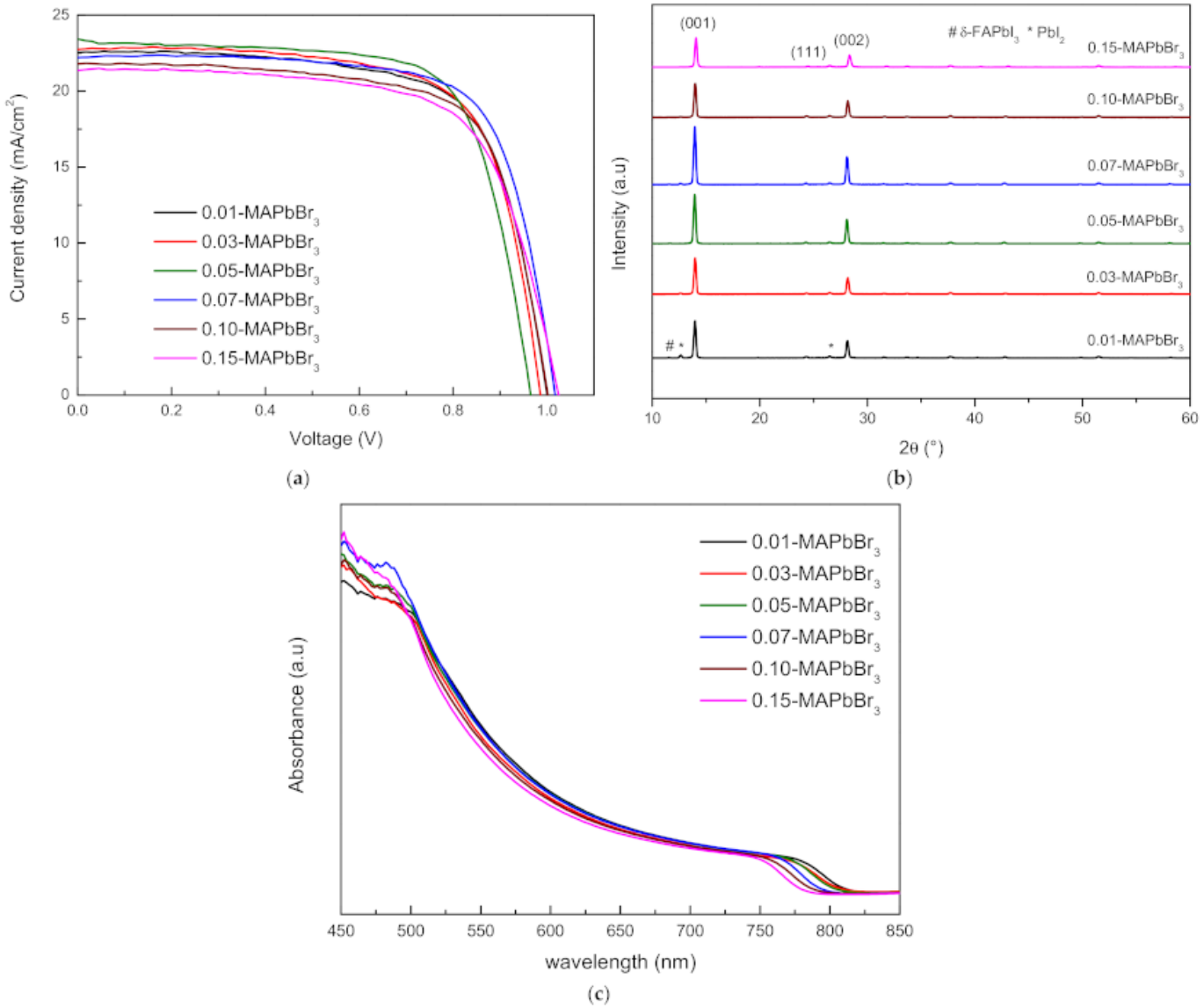

Figure 2. (**a**) Photocurrent density-voltage curve of the X-MAPbBr$_3$ based PSCs. (**b**) XRD patterns of the X-MAPbBr$_3$ perovskite film. (**c**) UV-vis absorption spectra of the X-MAPbBr$_3$ film.

Table 2. Photovoltaic parameters of the best-performing X-MAPbBr$_3$ PSCs.

Sample	V_{OC}	J_{SC}	FF	PCE (%)	Rs(Ω)
0.01-MAPbBr$_3$	1.000	22.538	69.594	15.691	120.472
0.03-MAPbBr$_3$	0.986	22.729	70.188	15.730	113.333
0.05-MAPbBr$_3$	0.965	23.407	70.878	16.014	109.144
0.07-MAPbBr$_3$	1.017	22.196	72.176	16.301	116.721
0.10-MAPbBr$_3$	1.002	21.785	70.414	15.372	122.829
0.15-MAPbBr$_3$	1.025	21.651	67.764	14.826	147.174

3.3. FAPbI$_3$-FAPbBr$_3$ Perovskite Solar Cells

Figure 3a shows the J-V curve of the $(FAPbI_3)_{1-X}(FAPbBr_3)_X$ perovskite (renamed X-FAPbBr$_3$) device with 40 mol% MACl. A summary of the photovoltaic properties of X-FAPbBr$_3$ is presented in Table 3. Surprisingly, despite the very small composition ratio of FAPbBr$_3$, the 0.01-FAPbBr$_3$ film exhibited an outstanding PCE of 16.569% with a V_{OC} of 1.016 V, a J_{SC} of 23.413 mA·cm^{-2}, and an FF of 69.622%. The enhanced V_{OC}

of 1–15-$FAPbBr_3$ can be attributed to the increase in the bandgap and the decrease in the electron-hole recombination at the interface between the perovskite film and the hole transport layer and electron transport layer [20,21]. Figure 3b shows the XRD pattern of the X-$FAPbBr_3$ perovskite film. The 2θ peaks at 13.95°, 26.50°, and 28.12° in the XRD patterns confirm the existence of α-$FAPbI_3$ in the fabricated perovskite film. The XRD pattern confirmed that the 0.01-$FAPbBr_3$ film had the highest crystallinity. Thereafter, when increasing the amount of $FAPbBr_3$, the intensity of the perovskite peak decreased. As with X-$MAPbBr_3$, it was confirmed that as the composition ratio of $FAPbBr_3$ increased, the diffraction peak of the (001) plane shifted to a larger angle [22]. Figure 3c shows the absorbance of the X-$FAPbBr_3$ perovskite film. The 0.01-$FAPbBr_3$ film had the highest absorbance. Subsequently, the absorbance gradually decreased as the $FAPbBr_3$ content of the X-$FAPbBr_3$ film increased. These results are responsible for the progressive decrease in J_{SC} with an increasing concentration of $FAPbBr_3$ (Table 2) [23]. In the 750–850 nm wavelength range, the absorbance of the X-$FAPbBr_3$ film blue-shifted with increasing $FAPbBr_3$, which has a wider bandgap similar to X-$MAPbBr_3$.

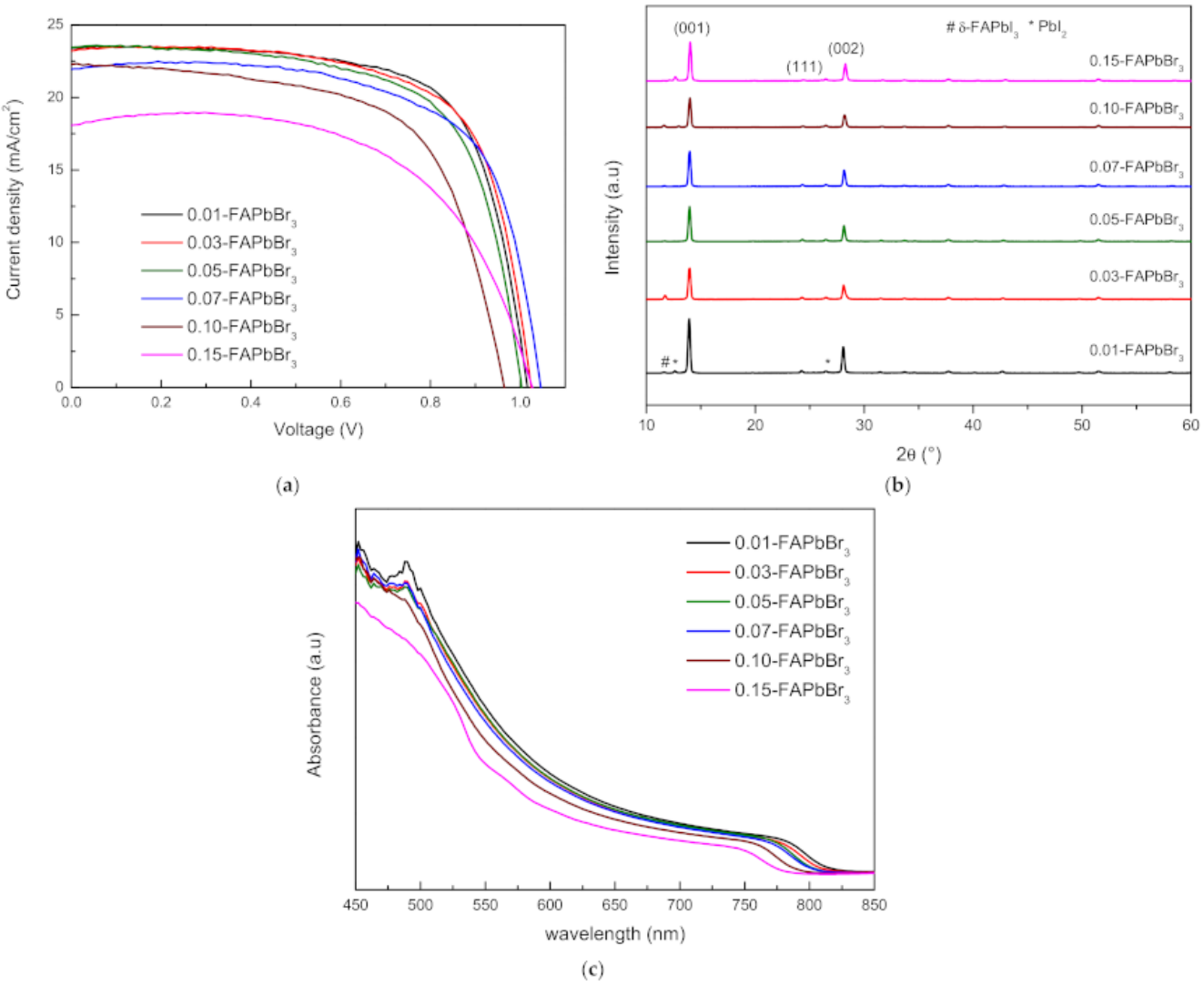

Figure 3. (**a**) Photocurrent density-voltage curve of the X-$FAPbBr_3$ based PSCs. (**b**) XRD patterns of the X-$FAPbBr_3$ perovskite films. (**c**) UV-vis absorption spectra of the X-$FAPbBr_3$ film.

Table 3. Photovoltaic parameters of the best-performing X-$FAPbBr_3$ PSCs.

Sample	V_{OC}	J_{SC}	FF	PCE (%)	Rs (Ω)
0.01-$FAPbBr_3$	1.016	23.413	69.622	16.569	117.628
0.03-$FAPbBr_3$	1.025	23.221	68.781	16.364	115.223
0.05-$FAPbBr_3$	1.003	23.481	66.948	15.766	123.569
0.07-$FAPbBr_3$	1.045	21.938	67.446	15.468	126.702
0.10-$FAPbBr_3$	0.965	22.275	62.861	13.508	153.506
0.15-$FAPbBr_3$	1.027	18.055	60.814	11.274	231.911

3.4. Comparison of $FAPbI_3$-$FAPbBr_3$ and $FAPbI_3$-$MAPbBr_3$ Perovskite Solar Cells

In Table 4, the difference between R_S and FF of the optimized composition of $FAPbI_3$-$MAPbBr_3$ and $FAPbI_3$-$FAPbBr_3$ perovskite solar cells was not significant, indicating that the manufactured cells had similar stability [24,25]. Figure 4a,b shows the surface image of the perovskite films. The average grain sizes of 0.01-$FAPbBr_3$ and 0.07-$MAPbBr_3$ were approximately 769 nm and 652 nm, respectively. The difference in grain size between 0.01-$FAPbBr_3$ and 0.07-$MAPbBr_3$ affects J_{SC} based on the difference in light absorption. [26]. Figure 4c is a cross-sectional SEM image of PSCs without the top electrode. The thickness of TiO_2/perovskite/Spiro-OMeTAD is 240 nm, 348 nm, and 244 nm, respectively. As shown in Figure 5a, the J_{SC} difference between 0.01-$FAPbBr_3$ and 0.07-$MAPbBr_3$ is clearly visible. This is considered to be due to the difference in the grain size, as mentioned above [27]. In addition, 0.01-$FAPbBr_3$ shows reduced hysteresis compared to 0.07-$MAPbBr_3$. The hysteresis index (HI, listed in Table 4) was extracted using the equation in [28]. The 0.07-$MAPbBr_3$ device showed a significant PCE difference between 14.745% (forward) and 16.301% (reverse). The 0.01-$FAPbBr_3$ device has a low hysteresis effect with PCEs of 16.569% and 15.656% for the reverse and forward directions, respectively. That is, the HI decreased from 0.095 to 0.055. The normal distribution model was applied to the histogram shown in Figure 5b. Both histograms show that the 0.01-$FAPbBr_3$-based device exhibited improved solar cell performance compared to the 0.07-$MAPbBr_3$-based device.

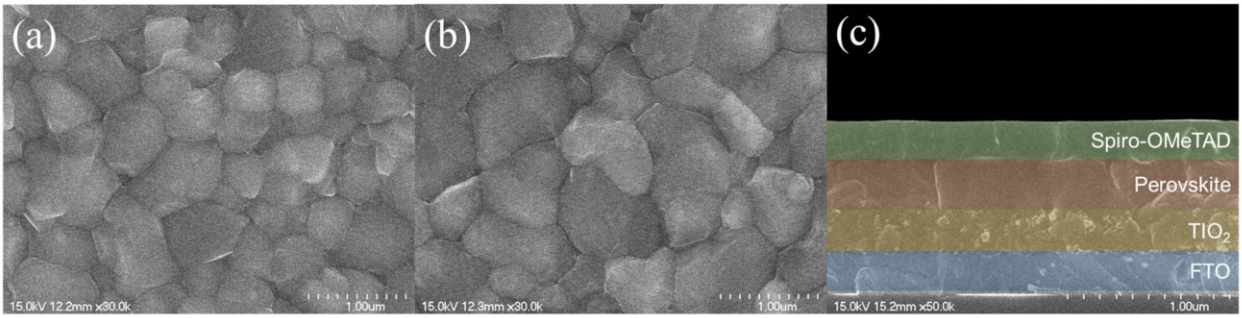

Figure 4. The surface FE-SEM images of (**a**) the 0.07-$MAPbBr_3$ and (**b**) 0.01-$FAPbBr_3$ perovskite film. (**c**) Cross-sectional FE-SEM images of the PSC.

Table 4. Photovoltaic parameters of the best-performing X-$FAPbBr_3$ PSCs.

Sample	Sweep Direction	V_{OC}	J_{SC}	FF	PCE (%)	R_S(Ω)	HI
0.01-$FAPbBr_3$	FS	1.001	23.425	66.797	15.656	132.024	0.055
	RS	1.016	23.413	69.622	16.569	117.628	
0.07-$MAPbBr_3$	FS	0.983	21.833	68.702	14.745	143.729	0.095
	RS	1.017	22.196	72.176	16.301	116.721	

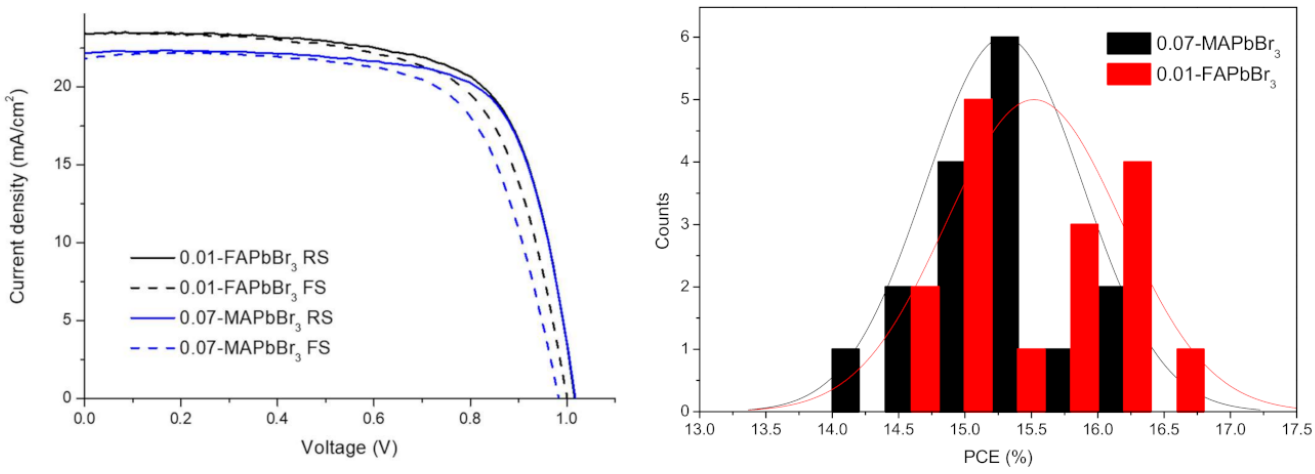

Figure 5. (**a**) Forward and reverse scans current density-voltage curve of the 0.07-$MAPbBr_3$ and 0.01-$FAPbBr_3$ based PSCs (hysteresis effect). (**b**) PCE distribution of the 32 PSCs.

4. Conclusions

In this study, the addition amount of MACl was first optimized to reduce the dependence of $MAPbBr_3$ or $FAPbBr_3$ on the phase stability enhancement of $FAPbI_3$. The 40-MACl device had a champion PCE of 15.379%, and 40 mol% MACl addition was adopted for the $FAPbI_3$-$MAPbBr_3$ and $FAPbI_3$-$FAPbBr_3$ films. $MAPbBr_3$ or $FAPbBr_3$ not only accelerated the δ to α phase transformation process of the $FAPbI_3$ perovskite film, but also improved the crystallinity and formed a uniform perovskite film. Among the $FAPbI_3$-$MAPbBr_3$ PSCs, the 0.07-$MAPbBr_3$ device had the highest PCE of 16.301% and higher photovoltaic performance than the commonly used 0.10- and 0.15-$MAPbBr_3$ devices. Among the $FAPbI_3$-$FAPbBr_3$ devices, 0.01-$FAPbBr_3$ showed the PCE of 16.569% even with the lowest $FAPbBr_3$. Interestingly, the 0.01-$FAPbBr_3$ device, which was not adopted due to its low performance, was more efficient than the 0.07-$MAPbBr_3$ device and exhibited a suppressed hysteresis effect.

Author Contributions: Funding acquisition, H.W.C.; onvestigation, S.H.J.; supervision, H.W.C.; validation, H.W.C.; writing—original draft, S.H.J.; writing—review & editing, H.W.C. All authors have read and agreed to the published version of the manuscript.

Funding: This research was supported by the Basic Science Research Capacity Enhancement Project through the Korea Basic Science Institute (National Research Facilities and Equipment Center) grant funded by the Ministry of Education (2019R1A6C1010016). This work was supported by the Korea Institute of Energy Technology Evaluation and Planning (KETEP) and the Ministry of Trade, Industry & Energy (MOTIE) of the Republic of Korea (No. 20194030202290).

Institutional Review Board Statement: Not applicable.

Informed Consent Statement: Not applicable.

Data Availability Statement: Not applicable.

Conflicts of Interest: The authors declare no conflict of interest.

References

1. Han, Q.; Bae, S.H.; Sun, P.; Hsieh, Y.T.; Yang, Y.; Rim, Y.S.; Zhao, H.; Chen, Q.; Shi, W.; Li, G. Single crystal formamidinium lead iodide ($FAPbI_3$): Insight into the structural, optical, and electrical properties. *Adv. Mater.* **2016**, *28*, 2253–2258. [CrossRef] [PubMed]
2. Eperon, G.E.; Stranks, S.D.; Menelaou, C.; Johnston, M.B.; Herz, L.M.; Snaith, H.J. Formamidinium lead trihalide: A broadly tunable perovskite for efficient planar heterojunction solar cells. *Energy Environ. Sci.* **2014**, *7*, 982–988. [CrossRef]

3. Su, J.; Zheng, X.; Lang, X.; Han, R.; Cai, H.; Ni, J.; Zhang, J.; Qiu, J. Effect of precursor solution ageing time on the photovoltaic performance of perovskite solar cells. *Funct. Mater. Lett.* **2021**, *14*, 2151025. [CrossRef]
4. Koh, T.M.; Fu, K.; Fang, Y.; Chen, S.; Sum, T.C.; Mathews, N.; Mhaisalkar, S.G.; Boix, P.P.; Baikie, T. Formamidinium-containing metal-halide: An alternative material for near-IR absorption perovskite solar cells. *J. Phys. Chem. C* **2014**, *118*, 16458–16462. [CrossRef]
5. Zhang, T.; Xu, Q.; Xu, F.; Fu, Y.; Wang, Y.; Yan, Y.; Zhang, L.; Zhao, Y. Spontaneous low-temperature crystallization of α-$FAPbI_3$ for highly efficient perovskite solar cells. *Sci. Bull.* **2019**, *64*, 1608–1616. [CrossRef]
6. Yang, G.; Zhang, H.; Li, G.; Fang, G. Stabilizer-assisted growth of formamdinium-based perovskites for highly efficient and stable planar solar cells with over 22% efficiency. *Nano Energy* **2019**, *63*, 103835. [CrossRef]
7. Kim, M.; Kim, G.-H.; Lee, T.K.; Choi, I.W.; Choi, H.W.; Jo, Y.; Yoon, Y.J.; Kim, J.W.; Lee, J.; Huh, D. Methylammonium chloride induces intermediate phase stabilization for efficient perovskite solar cells. *Joule* **2019**, *3*, 2179–2192. [CrossRef]
8. Hanusch, F.C.; Wiesenmayer, E.; Mankel, E.; Binek, A.; Angloher, P.; Fraunhofer, C.; Giesbrecht, N.; Feckl, J.M.; Jaegermann, W.; Johrendt, D. Efficient planar heterojunction perovskite solar cells based on formamidinium lead bromide. *J. Phys. Chem. Lett.* **2014**, *5*, 2791–2795. [CrossRef]
9. Smecca, E.; Numata, Y.; Deretzis, I.; Pellegrino, G.; Boninelli, S.; Miyasaka, T.; La Magna, A.; Alberti, A. Stability of solution-processed $MAPbI_3$ and $FAPbI_3$ layers. *Phys. Chem. Chem. Phys.* **2016**, *18*, 13413–13422. [CrossRef]
10. Min, H.; Kim, M.; Lee, S.-U.; Kim, H.; Kim, G.; Choi, K.; Lee, J.H.; Seok, S.I. Efficient, stable solar cells by using inherent bandgap of α-phase formamidinium lead iodide. *Science* **2019**, *366*, 749–753. [CrossRef]
11. Bu, T.; Li, J.; Li, H.; Tian, C.; Su, J.; Tong, G.; Ono, L.K.; Wang, C.; Lin, Z.; Chai, N.; et al. Lead halide–templated crystallization of methylamine-free perovskite for efficient photovoltaic modules. *Science* **2021**, *372*, 1327–1332. [CrossRef]
12. Jeon, N.J.; Noh, J.H.; Yang, W.S.; Kim, Y.C.; Ryu, S.; Seo, J.; Seok, S.I. Compositional engineering of perovskite materials for high-performance solar cells. *Nature* **2015**, *517*, 476–480. [CrossRef]
13. Xie, F.; Chen, C.-C.; Wu, Y.; Li, X.; Cai, M.; Liu, X.; Yang, X.; Han, L. Vertical recrystallization for highly efficient and stable formamidinium-based inverted-structure perovskite solar cells. *Energy Environ. Sci.* **2017**, *10*, 1942–1949. [CrossRef]
14. Reyna, Y.; Salado, M.; Kazim, S.; Pérez-Tomas, A.; Ahmad, S.; Lira-Cantu, M. Performance and stability of mixed $FAPbI_{3(0.85)}$ $MAPbBr_{3(0.15)}$ halide perovskite solar cells under outdoor conditions and the effect of low light irradiation. *Nano Energy* **2016**, *30*, 570–579. [CrossRef]
15. Li, Y.; Zhang, T.; Xu, F.; Wang, Y.; Li, G.; Yang, Y.; Zhao, Y. CH_3NH_3Cl assisted solvent engineering for highly crystallized and large grain size mixed-composition $(FAPbI_3)_{0.85}(MAPbBr_3)_{0.15}$ perovskites. *Crystals* **2017**, *7*, 272. [CrossRef]
16. Mei, Y.; Liu, H.; Li, X.; Wang, S. Hollow TiO_2 spheres as mesoporous layer for better efficiency and stability of perovskite solar cells. *J. Alloys Compd.* **2021**, *866*, 158079. [CrossRef]
17. Mundhaas, N.; Yu, Z.J.; Bush, K.A.; Wang, H.P.; Häusele, J.; Kavadiya, S.; McGehee, M.D.; Holman, Z.C. Series resistance measurements of perovskite solar cells using Jsc–Voc measurements. *Sol. RRL* **2019**, *3*, 1800378. [CrossRef]
18. Isikgor, F.H.; Li, B.; Zhu, H.; Xu, Q.; Ouyang, J. High performance planar perovskite solar cells with a perovskite of mixed organic cations and mixed halides, $MA_{1-x}FA_xPbI_{3-y}Cl_y$. *J. Mater. Chem. A* **2016**, *4*, 12543–12553. [CrossRef]
19. Fang, H.-H.; Adjokatse, S.; Shao, S.; Even, J.; Loi, M.A. Long-lived hot-carrier light emission and large blue shift in formamidinium tin triiodide perovskites. *Nat. Commun.* **2018**, *9*, 1–8. [CrossRef] [PubMed]
20. Gharibzadeh, S.; Abdollahi Nejand, B.; Jakoby, M.; Abzieher, T.; Hauschild, D.; Moghadamzadeh, S.; Schwenzer, J.A.; Brenner, P.; Schmager, R.; Haghighirad, A.A. Record open-circuit voltage wide-bandgap perovskite solar cells utilizing 2D/3D perovskite heterostructure. *Adv. Energy Mater.* **2019**, *9*, 1803699. [CrossRef]
21. Correa-Baena, J.-P.; Tress, W.; Domanski, K.; Anaraki, E.H.; Turren-Cruz, S.-H.; Roose, B.; Boix, P.P.; Grätzel, M.; Saliba, M.; Abate, A. Identifying and suppressing interfacial recombination to achieve high open-circuit voltage in perovskite solar cells. *Energy Environ. Sci.* **2017**, *10*, 1207–1212. [CrossRef]
22. Slimi, B.; Mollar, M.; Assaker, I.B.; Kriaa, A.; Chtourou, R.; Marí, B. Synthesis characterization of perovskite $FAPbBr_{3-x}I_x$ thin films for solar cells. *Mon. Für Chem. -Chem. Mon.* **2017**, *148*, 835–844. [CrossRef]
23. Chen, L.-C.; Chen, J.-C.; Chen, C.-C.; Wu, C.-G. Fabrication and properties of high-efficiency perovskite/PCBM organic solar cells. *Nanoscale Res. Lett.* **2015**, *10*, 1–5. [CrossRef]
24. Bao, X.; Wang, Y.; Zhu, Q.; Wang, N.; Zhu, D.; Wang, J.; Yang, A.; Yang, R. Efficient planar perovskite solar cells with large fill factor and excellent stability. *J. Power Sources* **2015**, *297*, 53–58. [CrossRef]
25. Krishnan, U.; Kaur, M.; Kumar, M.; Kumar, A. Factors affecting the stability of perovskite solar cells: A comprehensive review. *J. Photonics Energy* **2019**, *9*, 021001.
26. Kim, H.D.; Ohkita, H.; Benten, H.; Ito, S. Photovoltaic performance of perovskite solar cells with different grain sizes. *Adv. Mater.* **2016**, *28*, 917–922. [CrossRef] [PubMed]
27. Gedamu, D.; Asuo, I.M.; Benetti, D.; Basti, M.; Ka, I.; Cloutier, S.G.; Federico, R.; Nechache., R. Solvent-antisolvent ambient processed large grain size perovskite thin films for high-performance solar cells. *Sci. Rep.* **2018**, *8*, 1–11. [CrossRef] [PubMed]
28. Habisreutinger, S.N.; Noel, N.K.; Snaith, H.J. Hysteresis index: A figure without merit for quantifying hysteresis in perovskite solar cells. *ACS Energy Lett.* **2018**, *3*, 2472–2476. [CrossRef]